Chemical and Green Synthesis of CuO Nanoparticles using *Carica Papaya* Leaf Extract: Structural and Optical properties

Ingalagondi P K[1,a], K Mruthunjaya[2], S M Hanagodimath[3], N C Horti[4,b]

[1] *Department of Physics, Government First Grade College for Women, Davanagere-570 004, Karnataka, India.*
[2] *Department of Pharmacognosy, JSS College of Pharmacy, Academy of Higher Education and Research, Mysuru-570 015, Karnataka, India.*
[3] *Department of Physics, Gulbarga University, Kalaburagi – 585 106, Karnataka, India.*
[4] *Department of Physics, S.S. Government First Grade College and P.G Study Centre, Nargund -582 207, Karnataka, India.*

[a] ings744@gmail.com
[b] ningappa.c.horti@gmail.com

Abstract

This article describes the synthesis of CuO nanoparticles through a two different synthesis routes, namely a chemical co-precipitation and green synthesis route using *Carica papaya* leaf extract and their optical properties. The samples were investigated for their structural and optical properties through X-ray diffraction, scanning electron microscopy, Fourier transfer infrared, UV absorption, photoluminescence and time resolved spectroscopy. The XRD spectra of both samples demonstrate the CuO crystallizes in a monoclinic phase with particle sizes ranging from 20-25 nm. SEM pictures of samples showed the highly agglomerated and spherical particles are formed. The peaks in FTIR spectra are located between 600-1000 cm^{-1}, confirming the formation of CuO phase. The observed shift in UV absorption edge and PL peak of both samples is the result of size quantization and various surface defects. The carrier life time study of both samples revealed the recombination rate of exciton depend on particle size and surface defects. The results of this study indicates CuO is an alternative material for solar cell and optoelectronic devices.

Keywords: Copper oxide, *Carica papaya* leaf extract, Chemical and Green synthesis, Optical properties, Time resolved spectroscopy.
Received 27 January 2025; First Review 02 February 2025; Accepted 07 February 2025

*** Address of correspondence**
Dr. N C Horti
Department of Physics, S.S. Government First Grade College and P.G Study Centre, Nargund - 582 207, Karnataka, India.

Email: ningappa.c.horti@gmail.com

How to cite this article
Ingalagondi P K, K Mruthunjaya, S M Hanagodimath, N C Horti, Chemical and Green Synthesis of CuO Nanoparticles using Carica papaya leaf Extract: Structural and Optical properties, J. Cond. Matt. 2024; 02 (02):12-19.

Available from:
https://doi.org/10.61343/jcm.v2i02.62

Introduction

In recent years, metal oxide (CuO, NiO, ZnO, SnO_2 and TiO_2) nanoparticles have gained a main research focus due to their remarkable properties and diversified applications [1-3]. Among these, copper oxide presents in two phases; CuO (Cupric Oxide) and Cu_2O (Cuprous oxide). CuO has a narrow band gap range of 1.2-1.55 eV and Cu_2O having a band gap of 2.1eV [4-5]. Among these two forms, CuO is a prospective material for photovoltaic devices because of its high absorbance coefficient and narrow band gap [6]. It also has a various applications like gas sensors [7], catalyst [8] lithium-ion batteries [9], magnetic storage devices [10] and high temperature superconductor [11]. The optical properties of CuO nanoparticles not only changes with size, capping agent, calcination temperature and solvents but also sensitive to the precursor used and synthesis route. The synthesis technique could effect on optical properties of CuO nanostructures because of its different oxidation states (CuO, Cu_2O, Cu_2O_3) and size/shape [12]. Although there is a numerous article on the synthesis and optical properties but a lack of attention paid to photo-physical performance of green synthesized CuO nanoparticles using *Carica papaya* leaf extract.

Due to the advancement of nanotechnology, there are now a variety of synthesis routes available to synthesize nanoparticles, including sol-gel [13], hydrothermal [14], chemical co-precipitation [15], solution combustion [16], solid state method [17] and green synthesis route [18-19]. Among them, green synthesis route is an important and cost-effective method as compared to the above-mentioned methods. Moreover, it is an eco-friendly. There are some disadvantages of chemical synthesis routes including that of hazardous starting materials and generation of toxic by-products [20]. Therefore, researchers are motivated to

synthesize nanoparticles through a green synthesis processes using various plant extract. Chan *et al* [21] have developed the CuO nanostructures via green synthesis route using *Garcinia mangostana L.* leaf extract. They noticed the redshift of absorption edge with an increasing calcination temperature due to the aggregation and the growth of particles. Using copper acetate as copper source and *Caloropis procera* leaf extract, Reddy *et. al.* [22] fabricated the CuO nanoparticles through green synthesis route. They found the band gap to be 2.35 eV. Gunalan and his group [23] have synthesized CuO nanoparticles through a chemical and biological route using *Aloe Vera* leaf extract. In their absorption study, they noticed the peaks around at 265 nm and 285 nm due to the surface plasmon resonance and noticed the PL peak around at 600 nm due to the singly ionized oxygen vacancies. Sackey and co-workers [24] have reported the biosynthesis of CuO nanoparticles by employing aqueous extract of Mimosa hamate. They found the band gap around 1.5 eV from diffuse reflectance spectra analysis and antibacterial activities were also studied. A biogenic synthesis of rice shaped CuO nanoparticles via aqueous extract of *Caesalpinia bonducella* seed was reported by Sukumar *et. al.* [25]. They noticed peak at 250 nm in UV absorption spectra due to the surface plasmon resonance and broad peak from 320 nm-600 nm due to the non-oxidized Cu ions. Very recently, bio-synthesis of CuO nanoparticles using *white garland Lily* Leave extract was reported by Nagore *et. al.* [26]. They noticed the absorption edge at 300 nm due to the recombination of exciton and the green-yellow emission at 590 nm. In all of these studies, the CuO have been synthesized by green synthesis route and the optical properties was altered as a result of particle aggregation, singly ionized oxygen vacancies, and non-oxidized Cu ions. The improved optical properties of CuO, making it a unique material for number of scientific and technological applications. A few studies on optical properties of green synthesized CuO nanoparticles have been reported in literature, however optical properties including carrier life time measurement of green synthesized CuO nanoparticles using *Carica papaya* leaf extract have not been thoroughly explored. Furthermore, no studies have been published on comparing optical properties of chemically and green synthesized CuO nanoparticles. In addition, *Papaya* (*Carica papaya L*) is one of the most important medicinal plant and its different parts such as leaves, roots, fruit, flowers, and seeds are used for the treatment to varieties of diseases namely few; diabetes, cancer, heart stroke, blood pressure and many other. They contain the various constituents, including vitamins B, C and E and rich in minerals (Fe, Na and Ca), antioxidants and fibres. Moreover, it is a good as reducing and stabilizing agent. Therefore, in this work we report the chemical and green synthesis of CuO nanoparticles using *Carica papaya* leaf extract and chemical co-precipitation method using $CuSO_4.5H_2O$ as a copper source and the structural and optical properties are investigated.

Materials and Method

SD fine chemicals Pvt Ltd supplied Copper sulphate pentahydrate ($CuSO_4.5H_2O$), Sodium hydroxide (NaOH) pellets, Ethanol (HPLC grade) and *Papaya* (*Carica papaya L*) leaf extract.

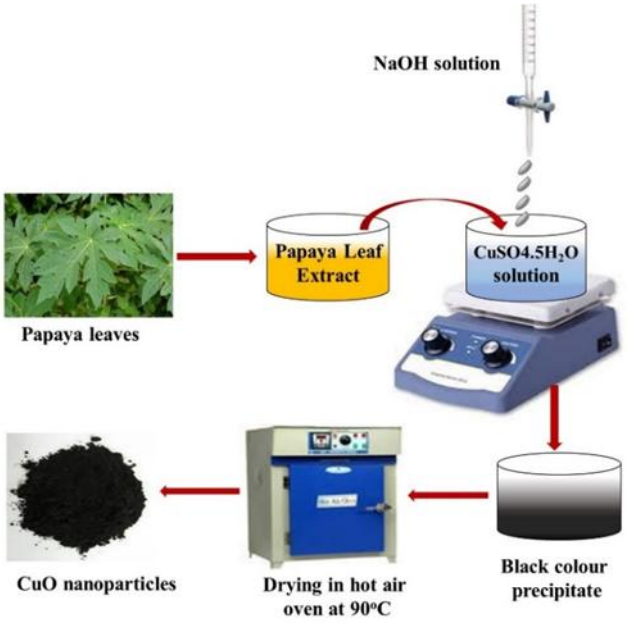

Figure 1: Flow diagram of green synthesis of CuO nanoparticles.

Chemical synthesis of CuO nanoparticles

In chemical synthesis of CuO nano powder, the preparation of $CuSO_4.5H_2O$ (2.496 gm) and NaOH (0.8 gm) solutions were prepared in 50 ml and 20 ml of de-ionized water, respectively. Then, the addition of prepared NaOH solution drop-by drop to $CuSO_4.5H_2O$ solution. During reaction, the black color $Cu(OH)_2$ precipitate was formed. The black-colored precipitate was filtered and washed thoroughly for 3-4 times using ethanol and de-ionized water to purify the product. Then, the powder was heated at 90 °C in hot air oven before being calcined at 500 °C in muffle furnace for two hours.

Preparation of *papaya* leaf extract

Carica papaya leaves were collected from local garden of Gulbarga University, Kalaburagi. India. The collected papaya leaves (20 gm) were washed 3-4 times with de-ionized water to eliminate dust particles. Using domestic mixture, the cleaned *papaya* leaves were grinded and heated in 100 ml of deionized water for two hours. After two hours of heating, the pale yellow colour solution was found and filtered using Whatman paper. Thereafter, the leaf extract was stored in 5 °C till use for next synthesis.

Green synthesis of CuO nanoparticles

In procedure of green synthesis, the solution of $CuSO_4.5H_2O$ was prepared in 50 ml of de-ionized water and treated with 20 ml of prepared *papaya* leaf extract and stirred for an hour. pH of the mixture solution was maintained 7 by adding 0.1M NaOH solution and a black colored precipitate was appeared. The resulted precipitate was washed repeatedly using ethanol and de-ionized water to purify the product. At last, the sample was calcined at 500 °C for two hours in muffle furnace. The flow diagram for green synthesis of CuO nanoparticles is shown in figure 1. Here, we indicated the chemically synthesized sample as S_1 and the green synthesized sample as S_2.

Characterization methods

To collect XRD data of samples, Smart Lab SE, Rigaku X-ray diffractometer with CuKα radiation of wavelength (0.15406 nm) was used. Surface morphology and size distribution of samples were analyzed through MIRA3 LMH TESCAN scanning electron microscopy. Nicolet-6900, FTIR spectrophotometer was utilized to confirm the formation of CuO nanoparticles. UV absorption measurement of samples were carried out by JASCO, V-670 UV–Vis absorption spectrophotometer. Fluorescence emission spectra were recorded using Hitachi, F-7100 spectrophotometer and Chronos BH, ISS spectrofluorometer was used to record the carrier lifetime of samples.

Results and discussion

XRD analysis

In figure 2 (a-b) we depict the X-ray diffraction pattern of sample S_1 and S_2, respectively. In the XRD pattern of both samples, all XRD peaks confirm the formation of monoclinic CuO phase and well coincides with JCPDS No-45-0937 [27-28]. The peaks at 2θ are 32.58°, 35.58°, 38.70°, 48.79°, 53.55°, 58.48°, 61.55°, 66.39°, 68.12°, 72.46°, 75.29° corresponding to planes (110), (002), (111), (-202), (020), (202), (-113), (022), (220), (-312) and (004) respectively. The sharp and narrow peaks of sample S_1 indicates high crystallinity and larger particle size as compared to sample S_2. No any characteristics peaks of $Cu(OH)_2$ and Cu_2O were observed, indicating the sample S_1 is crystalize in pure CuO with monoclinic phase. Some extra peaks were appeared in XRD spectrum of sample S_2 (Fig. b), which indicates the left overs of some minerals, vitamins and fibres of *papaya* leaf extract (indicated by asterisk). The particle size of samples was determined by adopting Scherrer formula and is given by [29]

$$D = \frac{K\lambda}{\beta Cos\theta} \qquad (1)$$

here D: particle size, β: FWHM of peak, λ: X-ray wavelength and θ being the glancing angle. The particle size S_1 sample is found to be 23.65 nm and that of sample S_2 is 16.37 nm.

For monoclinic structure, $a \neq b \neq c$, $\alpha = \gamma = 90°$ and $\beta > 90°$, the lattice parameters were calculated by following expression [30-31].

$$d_{hkl} = \left[\frac{\left(\frac{h^2}{a^2}\right)+\left(\frac{l^2}{c^2}\right)-\left(\frac{2hl}{ac}\right)cos\theta}{sin^2\beta} + \frac{k^2}{b^2}\right]^{-1/2} \qquad (2)$$

Where d_{hkl} : interplanar spacing. h, k and l: miller indices. The dislocation density was evaluated by equation (3)

$$\delta = \frac{1}{D^2} \qquad (3)$$

Where δ : dislocation density. The micro strain in lattice is caused by the presence of lattice imperfection and is calculated by [32]

$$\varepsilon = \frac{\beta}{4tan\theta} \qquad (4)$$

The usual meaning of term ε and β are the micro-strain and FWHM of peak, respectively. The values of estimated parameters are tabulated in table 1. It is noticed the difference in particle size and surface imperfections causes a change in the values of micro strain, dislocation density, and lattice parameters with different synthesis processes.

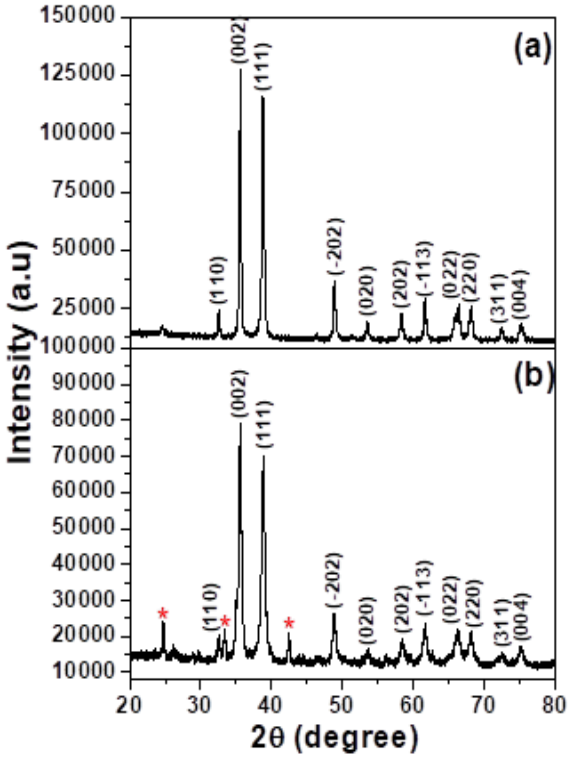

Figure 2: XRD spectrum of (a) S_1 and (b) S_2 sample.

Table 1: Estimated value of particle size, micro strain, dislocation density and lattice parameters of both samples.

Sample Name	Crystallite Size (nm)	Dislocation density (Lines/m^2) X 10^{15}	Microstrain (ε) X 10^{-3}	Lattice parameter (Å)		
				a	*b*	*c*
S_1	23.65	1.78	2.8	4.6893	3.4691	5.1327
S_2	16.37	3.73	5.1	4.6842	3.4237	5.1153

Morphological study

In figure 3(a-b) we show the morphological analysis of S_1 and S_2 sample, respectively. SEM image (a) shows the formation of highly agglomerated and spherical shaped particles are formed. The formation of irregular and agglomeration of particles were noticed from image (b), which indicates the change in reaction rate with various constituents of papaya leaf extract and remains of minerals of *papaya* leaf extract in the sample after washing.

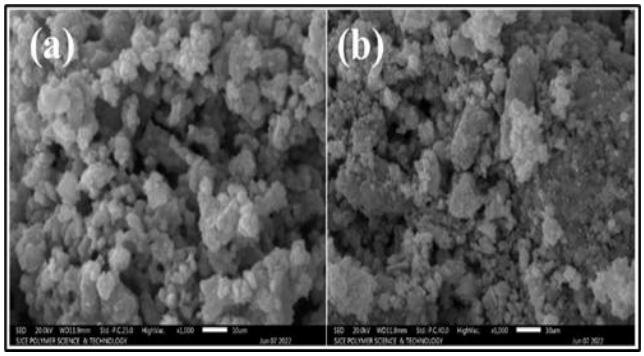

Figure 3: SEM images of (a) S_1 and (b) S_2 samples

Fourier Transform Infrared (FTIR) analysis

Figure 4 (a-b) shows the FTIR result of sample S_1 and S_2. In FTIR spectrum of sample S_1 (Fig. a), the peak at 517 cm^{-1} is assigned to the Cu-O mode of monoclinic phase [33-34]. The peak noticed at 1094 cm^{-1} due to the triply degenerative SO_4^{-2} vibration modes [35]. The band observed at 1384 cm^{-1} due to the vibration OH modes linked with copper atom [36]. The peaks at 1638 cm^{-1} and 3431 cm^{-1} are attributed to the –OH stretching/ bending vibration modes of adsorbed atmospheric moisture on surface of nanoparticles [37-38]. From FTIR spectrum of sample S_2 (Fig. b), the peaks noticed at 518 cm^{-1} and 610 cm^{-1} are corresponding to Cu-O vibration modes [39-40]. The peaks noticed around at 885 cm^{-1}, 1115 cm^{-1} and 2924 cm^{-1} are due to the vibration modes of various constituents of *papaya* leaf extract absorbed on particle surface [41-42]. The peak centered at 3483 cm^{-1} due to the vibration of hydroxyl group of water molecules [43].

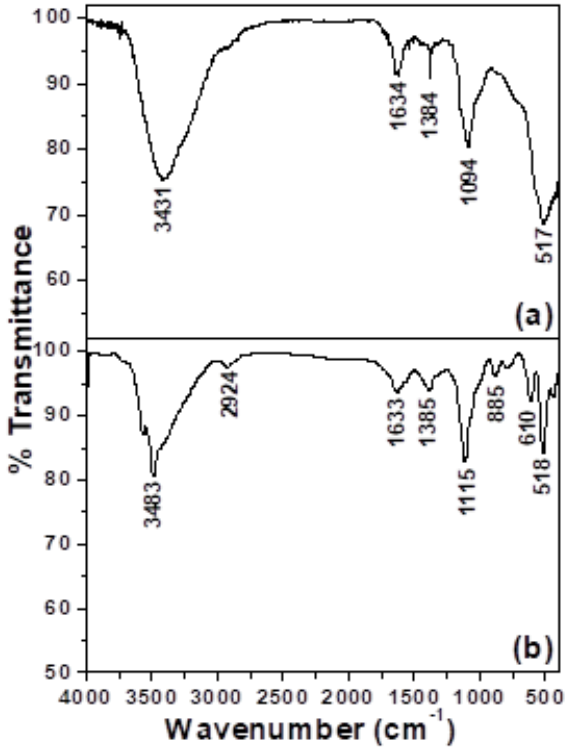

Figure 4 (a-b): FTIR spectra of sample S_1 and S_2.

UV-Visible absorption measurements

Figure 5(a-b) depict the UV-Vis absorption curve of sample S_1 and S_2, respectively. The absorption onset for the S_1 sample is noticed at 299 nm and that of sample S2 at 287 nm due to the direct charge transition from valence band to conduction band (O^{2-} to Cu^{2+} ion) [26,44]. The absorption edge of CuO nanoparticles depend on various factors like particle size, band gap, surface defects (oxygen vacancies) and synthesis techniques. The absorbance peak of sample S_2 is found at lower wavelength as compared to the S_1 sample which may ascribed to the smaller particle size.

Using Tauc relation, the energy gap of samples was evaluated [45,46] and is given by

$$(\alpha h\nu)^n = A(h\nu - E_g) \qquad (5)$$

Where, α: absorption coefficient, hν: photon energy and E_g: energy gap and the value of n is indicates the nature of

transition. In this case, we choose n = 2 for direct transition. In figure 6, we provided the Tauc plot of the samples S_1 and S_2. The energy gap is found to be 3.51 eV for the sample S_1 and that of sample S_2 is 3.57 eV. It is clearly noticed that the change in absorption edge and the value of energy band gap of samples with different synthesis routes due to the change in particle size and supported by XRD results. Furthermore, the obtained value of energy gap is greater than of bulk CuO and well matches with previously reported values of E_g by other researchers [47-48].

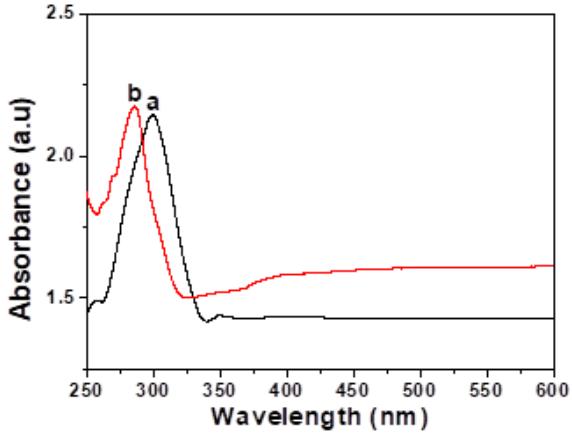

Figure 5: Absorption spectrum of sample S_1 (curve-a) and S_2 (curve-b).

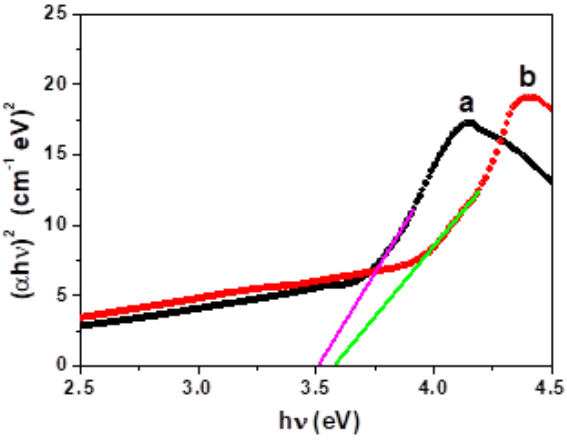

Figure 6: Tauc plot of sample (a) S_1 and (b) S_2.

Photoluminescence Study

Photoluminescence (PL) analysis is a significant tool for examining the optical emission of materials. The main sources of emission centers in metal oxides are oxygen vacancies and metal interstitials which varies with particle size, shape, composition and synthesis route [49]. PL spectra of CuO samples with different excitation wavelengths (400 nm, 410 nm, 420 nm, 430 nm) were recorded at room temperature and results are presented in figure 7 (a-b). The strong photoluminescence peak centred at 485 nm for the sample S_1 and that of sample S_2 at 472 nm due to the near band edge electron-hole recombination [50]. The peak position of sample S_1 shifted towards the higher wavelength as compared to S_2 sample, indicating the larger particle size of sample S_1 over sample S_2. The change in particle size with synthesis route due to the aggregation of particle in solution. When particles are reduced to the nanoscale, FL is influenced by many factors including a high surface area and surface imperfections. PL intensity of S_1 sample is a higher than of sample S_2 because of its larger particle size causes the decrease in number of surface defects which enhance the rate of exciton recombination [51]. Moreover, the weaker PL intensity of sample S_2 as compared to PL intensity of sample S_1 indicates the higher density of structural defects and impurities caused by remains of some minerals, vitamins and fibres of papaya leaf extract after sample washing, which is consistent with our XRD results. These surface imperfections promote the non-radiative recombination of electron-hole pairs, resulting in a drop in PL intensity. A notable shift of PL peak and PL intensity of samples with synthesis routes may be result of change in particle size and the presence of surface defects such as oxygen vacancies, metal interstitials and minerals of *papaya* leaf extract. The same behaviour was noticed by Das *et. al.* [52] for bio-synthesized CuO nanoparticles using *Madhuca longifolia* plant extract. It is concluded that the variation of PL properties depends of particle size and surface defects which may alter with synthesis routes.

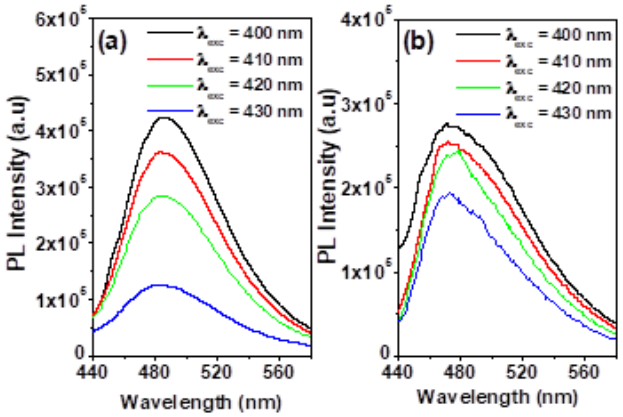

Figure 7 (a-b): Photoluminescence spectra of sample S_1 and S_2, respectively, with different excitation wavelength.

Time Resolved Spectroscopy

To know more information about particle size and surface defect related radiative electron hole recombination, Fluorescence (FL) life time measurement of samples were carried out by time co-related single photon counting system and results are given in figure 8(a-b). Fluorescence decay curves of CuO samples are well fitted with bi-exponential function and the value of χ^2 is nearly equal to a unity. FL decay of CuO depend on the various parameters including dopants, surface defects, solvent media and synthesis route. The synthesis methodology could affect the

carrier life time of materials due to the changes in surface defects and particle size. In present case, the decay curve of samples associated with direct recombination electron-hole pairs (fast decay) and the trapping of carriers in surface defects (slow decay) [53]. The value of τ_2 is smaller than τ_1 because of fast decay as a result of rapid radiative recombination of trap states electron after escaping from these states.

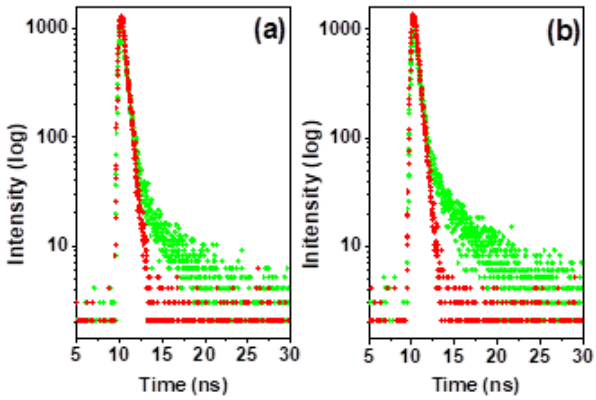

Figure 8(a-b): Fluorescence decay curves of samples S_1 and S_2, respectively.

Using fitted parameters, we have evaluated the average carrier life time of samples by following an expression [54].

$$\tau_{ave} = \frac{\sum_{i=1,2\ldots} A_i \tau_i^2}{\sum_{i=1,2\ldots} A_i \tau_i} \qquad (6)$$

Where, τ_{ave} represent the average carrier life time. A is the amplitude of decay curve. The obtained value of traced parameters and the average carrier life time of both samples are summarized in table 2. It is found that the sample S_2 has a longer average carrier life time than of sample S_1 ascribed to the trapping of charge carrier in surface defects and the smaller particle size. As a particle size increases, the average carrier life time increases due to the trapping of carrier in impurities by residual fibres and minerals of *papaya* leaf extract after washing. This is well consistent with our steady state fluorescence analysis and the particle size analysis XRD data. The density of oxygen vacancy and grain boundary are decreases with an increasing particle size causing short carrier life time [55]. This study highlights the variation of carrier lifetime of samples with synthesis techniques due to the trapping of carriers in surface defects and change in particle size.

Conclusion

In summary, CuO nanoparticles have been synthesized through two distinct synthesis techniques, namely green synthesis and a chemical co-precipitation process. The structural and optical properties of samples were examined using XRD, SEM, FTIR spectroscopy, UV absorption, photoluminescence and time resolved spectroscopy. XRD pattern of samples revealed the appearance of CuO in monoclinic phase. SEM images display the highly agglomerated, irregular and spherical shaped particles are formed. The existence of peaks ranging from 600-1000 cm^{-1} in FTIR spectra confirms the formation of CuO monoclinic phase. From band gap estimation, the value of band gap is found to be 3.51 eV and 3.57 eV for the sample S_1 and S_2, respectively. From PL study, the sample S_1 shows the higher PL intensity than of S_2 sample because of its larger particle size and presence of various surface defect (oxygen vacancies and Cu ions) and well supported by carrier life time measurements. According to this study, CuO is the most suitable material for optoelectronic applications.

Acknowledgements

Authors thanks to SJCE polymer science and technology laboratory, Mysore, Karnataka, India for providing the facility of XRD and SEM characterization.

Table 2: Calculated value of fitted parameters and average carrier life time.

Sample Name	τ_1(ns)	τ_2 (ns)	A_1	A_2	τ_{ave} (ns)	χ^2
S_1	2.19	0.0215	0.107	0.893	2.02	1.03
S_2	3.11	0.0298	0.115	0.885	2.89	1.01

References

1. N. C. Horti, M. D. Kamatagi, N. R. Patil, S. K. Nataraj, M. S. Sannaikar and S. R. Inamdar, Optik.194:163070, 2019.
2. P. K. Ingalagondi, N. C. Horti, Y. T. Ravikiran, M. Prashantkumar and B. G. Kumaraswamy, Chem Papers. 78:3331–3342, 2024.
3. N. C. Horti, M. D. Kamatagi, S. K. Nataraj, M. S. Sannaikar, and S. R. Inamdar, AIP Conf.Proc.2274: 020002, 2020.
4. K. Khojier, H. Savaloni and Z. Sadeghi, J.

Theoretical & Appl. Phys. 8:116, 2014.
5. W. J. Lee and X. J. Wang, Coatings. 11:864, 2021.
6. K. Das, S. N. Sharma, M. Kumar and S. K. De, J. Appl. Phys. 107:024316, 2010.
7. S. Sharma, K. Kumar, N. Thakur, S. Chauhan and M. S. Chauhan, J. Environ. Chem. Engineer. 9:105395, 2021.
8. J. C. Yan, W. Tianyi, M. Y. Liu and Z. Yuan, J. Nat. Ga. Chem. 20:669-676, 2011.
9. X. P. Gao, J. L. Bao, G. L. Pan, H. Y. Zhu, P. X. Huang, F. Wu and D. Y. Song, 108: 5547–5551, 2004.
10. R. A. Borzi, S. J. Stewart, R. C. Mercader, G. Punte and F. Garcia, J. Magnetism & Magnetic Mater. 226–230:1513–1515, 2011.
11. I. Y. Erdogana and O. Gullub, J. Alloys. Comp, 492: 378–383, 2010.
12. M. Censabella, V. Iacono, A. Scandurra, K. Moulaee, G. Neri, F. Ruffino, S. Mirabella, Sensors and Actuators B: Chemical. 358:131489, 2022.
13. F. Wang, H. Li, Zyaan, Y. Sun, F. Chang, H. Deng, L. Xie and H. Li, RSC Advan, 6: 79343-79349, 2016.
14. M. Chandrasekar, M. Subash, S. Logambal, G. Udhayakumar, R. Uthrakumar, C. Inmozhi, W. A. Al-Onazi, A. M. Al-Mohaimeed, T. W. Chen and K. Kanimozhi, J. King Saud Univer - Sci, 34: 101831, 2022.
15. N. C. Horti, M. D. Kamatagi, N. R. Patil, M. N. Wari, and S. R. Inamdar, Optik, 169: 314-320, 2018.
16. M. R. Islam, J. E. Obaid, M. Saiduzzaman, S. S. Nishat, T. Debnath and A. Kabir, J. Phys. Chem. Solids, 147: 109646, 2020.
17. N. C. Horti, M. D. Kamatagi and S. K. Nataraj, AIP Confer. Proceed., 2100, 020048, 2019.
18. R. Chowdhury, A. Khan and M. H. Rashid, RSC Advan, 10:14374-14385, 2020.
19. Z. Alhalili, Arabian J. Chem. 15: 103739 2022.
20. Ishwarya M. S, N. C. Horti, M. D. Kamatagi and Lokesh. S, 8: 717- 725, 2021.
21. Y. B. Chan, V. Selvanathan, L. H. Tey, M. Akhtaruzzaman, F. H. Anur, S. Djearamane, A. Watanabe and M. Aminuzzaman, Nanomaterials, 12: 3589, 2022.
22. K. Rayapa Reddy, J. Mole. Stru, 1150: 553-557, 2017.
23. S. Gunalan, R. Sivaraj and R. Venckatesh, Spectrochimica Acta Part A, 97: 1140–1144 (2012).
24. J. Sackey, L. C. Razanamahandry, S. K. O. Ntwampe, N. Mlungisi, A. Fall, C. Kaonga, and Z. Y. Nuru, Mater. Today: Proc. 36:540-548, 2021.
25. S. Sukumar, A. Rudrasenan and D. P. Nambia, ACS Omega. 5: 1040–1051, 2020.
26. P. B. Nagore, A. J. Ghoti, A. P. Salve and K. G. Mane, Bio. Nano. Sci. 12: 1086–1096 2022.
27. C. Jing, C. J. Yan, X. T. Yuan and L. P. Zhu, J. Photochem. Photobio B: Bio. 198: 111557, 2019.
28. D. P. Volanti, D. Keyson, L. S. Cavalcante, A. Z. Simoes, M. R. Joya, E. Longo, J. A. Varela, P. S. Pizani and A. G. Souza, J. Alloys. Comp. 459: 537–542, 2008.
29. N. C. Horti, A. Samage, M. A. Halakarni, S. K. Chavan, S. R. Inamdar, M. D. Kamatagi and S. K. Nataraj, Mater. Chem. Phys. 318:129276, 2024.
30. R. Javed, M. Ahmed, I. Haq, S. Nisa, M. Zia, Mater. Sci & Eng: C, 79:108-115, 2017.
31. S. Sharma, K. Kumar, N. Thakur, S. Chauhan, M. S. C hauhan, J. Environ. Chem. Eng, 9: 105395, 2021.
32. D.U.Beelagi, N.C.Horti and M.D.Kamatagi, J. Phys.:Conf.Ser. 2603: 012001, 2023.
33. K. K. Sahu, B. Raj, S. Basu and M. Mohapatra, ACS Omega, 6: 1108−1118, 2021.
34. E. Bharathi, G. Sivakumari, J. Kamalakkannan, B. Karthikeyan and S. Senthilvelan, Mater. Sci. Ene. Tech, 3: 407- 419, 2020.
35. N. C. Horti, M. D. Kamatagi, N. R. Patil, M. S. Sannaikar and S. R. Inamdar, J. Nanophoton, 14: 046010, 2020.
36. K. Phiwdang, S. Suphankij, W. Mekprasart and W. Pecharapa, Energy Procedia, 34:740-745, 2013.
37. P. Chand, Manisha and P. Kumar, Optik, 156:743-753, 2018.
38. M. S. Jagadeesan, K. Movlaee, T. Krishnakumar, S. G. Leonardi and G. Neri, J. Electroanal. Chem, 835:161-168, 2019.
39. J. K. Sharma, M. S. Akhtar, S. Ameen, P. Srivastava and G. Singh, J. Alloys. Comp. 632: 321-325, 2015.
40. A. Santha, Rintu Varghese, H. Joy Prabu, I. Johnson, D. Magimai Antoni Raj and S. John Sundaram, Mater. Today: Proc. 36: 447- 452, 2021.
41. S. H. Sabeeh, H. A. Hussein and H. K. Judran, Mater. Res. Express. 3: 125025, 2016.
42. G. Sharmila, R. Sakthi Pradeep, K. Sandiya, S. Santhiya, C. Muthukumaran, J. Jeyanthi, N. Manoj Kumar and M. Thirumarimurugan, J. Mole. Stru. 1165: 288-292, 2018.
43. E. Nagaraj, K. Karuppannan, P. Shanmugam and S. Venugopal, J. Cluster. Sci. 30: 1157–1168, 2019.
44. P. Nagore, S. Ghotekar, K. Mane, A. Ghoti, M. Bilal, A. Roy, Bio-Nano Science. 11: 579 - 589, 2021.
45. J. Tauc, A. Menth, J. Non-Crystalline Solids, 8-10: 569–585, 1972.
46. N. C. Horti, M. D. Kamatagi, N. R. Patil, S. K. Nataraj, S. A. Patil and S. R. Inamdar, Polym.Bull, 78: 6321-6336, 2021.
47. Z. R. Parekh, S. H. Chaki, A. B. Hirpara, G. H. Patel, R. M. Kannaujiya, A.J. Khimani, and M. P. Deshpande, Physica B: Conden. Matter, 610: 412950, 2021.
48. M. B. Mobarak, M. S. Hossain, F. Chowdhury and

S. Ahmed, Arabian J. Chem, 15: 104117, 2022.
49. W. Ding, D. Liu, J. Liu, J. Zhang, Chinese Journal of Chemistry, 38: 1832-1846, 2020.
50. A. El-Trass, H. ElShamy, I. El-Mehasseb and M. El-Kemary, Appl. Sur. Sci, 258: 2997- 3001, 2012.
51. H. Siddiqui, M. S. Qureshi and F. Z. Haque, Optik, 125: 4663-4667, 2014.
52. P. Das, S. Ghosh, R. Ghosh, S. Dam and M. Baskey, J. Photochem. Photobio. B: Bio. 189: 66-73, 2018.
53. A. D. Pramata, K. Suematsu, A. T. Quitain, M. Sasaki, and T. Kida, Advan. Fun. Mater, 28: 1704620, 2017.
54. N. C. Horti, M. D. Kamatagi, S. K. Nataraj, M. N. Wari and S. R. Inamdar, Nano Express, 1: 010022, 2020.
55. A. Seetharaman, D. Sivasubramanian, V. Gandhiraj, and V. R. Soma, J. Phys. Chem. C, 121: 24192-24205, 2017.